Cosmic voids as cosmological laboratories

C.M. Correa[1,2,3,4]

[1] *Max-Planck-Institut für Extraterrestrische Physik, Alemania*
[2] *Facultad de Matemática, Astronomía, Física y Computación, UNC, Argentina*
[3] *Instituto de Astronomía Teórica y Experimental, CONICET–UNC, Argentina*
[4] *Observatorio Astronómico de Córdoba, UNC, Argentina*

Contact / ccorrea@mpe.mpg.de

Resumen / Los relevamientos espectroscópicos modernos están cartografiando el Universo de una forma sin precedentes. En vista de ello, los vacíos cósmicos constituyen prometedores laboratorios cosmológicos. Existen dos estadísticas principales en los estudios de vacíos: (i) la función de tamaños, que cuantifica su abundancia, y (ii) la función de correlación cruzada vacío-galaxia, que caracteriza los campos de densidad y velocidad en sus alrededores. Sin embargo, para diseñar pruebas cosmológicas fiables basadas en estas estadísticas, es necesaria una descripción completa de los efectos de las distorsiones geométricas (efecto Alcock-Paczynski) y dinámicas (efecto Kaiser). Las mediciones observacionales muestran patrones anisótropos prominentes que conducen a ajustes cosmológicos sesgados si no se modelan adecuadamente. Presentaré un marco teórico para abordar esta problemática basado en un análisis cosmológico y dinámico del mapeo de vacíos entre el espacio real y el observado. Además, presentaré una nueva prueba cosmológica basada en dos proyecciones perpendiculares de la función de correlación, que no necesita suponer una cosmología fiduciaria, permite quebrar eficazmente degeneraciones en el espacio de parámetros del modelo y reducir significativamente el número de catálogos simulados necesarios para estimar covarianzas.

Abstract / Modern spectroscopic surveys are mapping the Universe in an unprecedented way. In view of this, cosmic voids constitute promising cosmological laboratories. There are two primary statistics in void studies: (i) the void size function, which quantifies their abundance, and (ii) the void-galaxy cross-correlation function, which characterises the density and velocity fields in their surroundings. Nevertheless, in order to design reliable cosmological tests based on these statistics, it is necessary a complete description of the effects of geometrical (Alcock-Paczynski effect) and dynamical (Kaiser effect) distortions. Observational measurements show prominent anisotropic patterns that lead to biased cosmological constraints if they are not properly modelled. I will present a theoretical framework to address this problematic based on a cosmological and dynamical analysis of the mapping of voids between real and redshift space. In addition, I will present a new fiducial-free cosmological test based on two perpendicular projections of the correlation function which allows us to effectively break degeneracies in the model parameter space and to significantly reduce the number of mock catalogues needed to estimate covariances.

Keywords / cosmological parameters — dark energy — distance scale — large-scale structure of universe

1. Introduction

In the last decades, we have entered a new era of high-precision cosmological measurements. Modern observations show that the Universe is not only expanding, it is also accelerating (Planck Collaboration et al., 2020). The standard model of Cosmology postulates a flat Λ-Cold Dark Matter (ΛCDM) Universe, in which this cosmic acceleration can be explained by the introduction of a new component known as dark energy, whose true nature we ignore. From a theoretical point of view, this component can be associated with the cosmological constant (Λ) in Einstein's field equations, also related with the vacuum energy. Alternatively, this could be a hint that we need to review our fundamental laws of gravity: General Relativity. Furthermore, dark energy is the current dominant component of the Universe: it contributes to almost 70% of the total energy budget. It is clear then that this dark-energy problem is one of the major challenges of modern Cosmology.

To date, there are three robust experiments that attest to the existence of a dark-energy component: (i) the Hubble diagram using distant supernovae Ia as standard candles (e.g. Suzuki et al., 2012), (ii) the study of the cosmic microwave background anisotropies (e.g. Planck Collaboration et al., 2020), and (iii) the Alcock-Paczynski tests using the baryon acoustic oscillations signal in the galaxy clustering as a standard ruler (e.g. Sánchez et al., 2013). In this sense, cosmic voids are alternative probes that can contribute to the study of dark energy from a different and independent point of view.

As matter clusters by the action of gravity, complementarily to this process, vast underdense regions are formed, the so-called cosmic voids. Roughly speaking, voids are regions with a density of 10 to 20% of the mean density of the Universe, and with sizes of tens of megaparsecs. However, the detailed statistical properties of the void population depend on two conditioning factors: (i) the type of matter tracers considered (e.g. galaxies in a spectroscopic survey, dark-matter particles in a simulation), and (ii) the method used to identify them from the spatial distribution of such tracers.

Why cosmic voids for Cosmology? In the first place, they are the largest observable structures. Therefore, they encode key information about the geometry and expansion history of the Universe. In this way, voids emerge as natural probes to test different dark-energy models. Secondly, their dynamics is less affected by non-linearities, allowing a simpler theoretical description. Furthermore, they constitute ideal environments for testing different modified gravity theories, mainly because of the unscreening mechanism that many of these models propose. Finally, the new generation of spectroscopic galaxy surveys, such as the Baryon Oscillation Spectroscopic Survey (Dawson et al., 2013, BOSS), Euclid (Laureijs et al., 2011), the Dark Energy Spectroscopic Instrument (Levi et al., 2019) or the Hobby-Eberly Telescope Dark Energy Experiment (Hill et al., 2008), are covering an unprecedented volume and redshift range. This will allow us to obtain rich samples of voids, and hence, to test the evolution history of the Universe with high precision.

In this article, I will summarise the main results of my PhD research about cosmic voids and their application as cosmological probes, already published in Correa et al. (2019, 2021, 2022) and Correa & Paz (2022). My PhD thesis is digitally available in Spanish at: `https://rdu.unc.edu.ar/handle/11086/21041`, and in English at: `https://doi.org/10.48550/arXiv.2210.17459`.

2. More about cosmic voids

2.1. The spherical void finder

There are many void finders in the literature, and equivalently, void definitions, each based on some fundamental properties of voids (e.g. Padilla et al., 2005; Neyrinck, 2008; Paz et al., 2022). A pragmatic choice is to use the definition that allows us to extract the greatest meaning in a given research context.

For the results presented in this work, we used the so-called spherical void finder developed by Ruiz et al. (2015), based on the original version of Padilla et al. (2005). Its essence lies in defining voids by calculating the integrated density contrast $\Delta(r)$ of underdense regions assuming spherical symmetry. The characteristics of this method make it ideal for the cosmological analyses that comprise this work.

Beyond the technicalities, the final output of the method is a catalogue of voids with the following characteristics: (i) each void object is an underdense spherical region, (ii) that do not overlap with other objects, (iii) with a well defined radius R_v and centre, (iv) from which an isotropic outflow of matter tracers is observed (in real space). Condition (iii) is satisfied by providing a threshold value $\Delta_{\mathrm{id}} = \Delta(R_v)$, motivated by the evolution of density perturbations, which is redshift dependent. In order to visualise how the void finder works, Fig. 1 shows a slice of the Millennium XXL simulation (Angulo et al., 2012, MXXL), where the spatial distribution of its dark-matter haloes and voids can be appreciated.
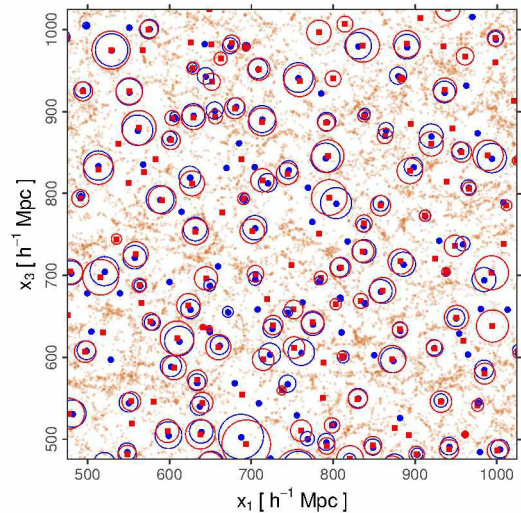

Figure 1: Slice of the MXXL simulation showing the line-of-sight spatial distribution of its dark-matter haloes and voids. Real-space voids are represented in blue; redshift-space voids, in red. The circles indicate the intersections of the spherical voids with the midplane of the slice. Figure credit: Correa et al. (2021).

2.2. Void statistics

There are two primary statistics in void studies: (i) the void size function (VSF), and (ii) the void-galaxy cross-correlation function (VGCF). The VSF (Sheth & van de Weygaert, 2004; Furlanetto & Piran, 2006; Jennings et al., 2013; Contarini et al., 2022; Paz et al., 2022), on the one hand, quantifies the comoving number density of voids as a function of their size. Hence, it characterises their abundance in the Universe. It is analogous to the mass function of dark-matter haloes. Therefore, it can be modelled in a similar fashion by means of the excursion set formalism combined with the spherical evolution of density perturbations. The VGCF (Paz et al., 2013; Cai et al., 2016; Hawken et al., 2020; Hamaus et al., 2020, 2022; Nadathur et al., 2020), on the other hand, quantifies the excess probability of finding void-galaxy pairs with respect to a homogeneous spatial distribution of such pairs. Hence, it characterises the density fluctuation field around voids. I will talk more about these statistics in the following sections.

The VSF and the VGCF are the cornerstones for the design of cosmological tests with cosmic voids. Essentially, the process consists on contrasting observational measurements of these statistics with physically-motivated model predictions in order to extract information about the cosmological parameters involved.

2.3. Spatial distortions

The measurement of the VSF and the VGCF basically depends on the spatial distribution of galaxies. However, this distribution is affected by the effect of spatial distortions, which translate into deviations and anisotropic patterns on the measurements. There are two main sources of spatial distortions. The first has

a geometrical origin, and is related to the selection of a fiducial cosmology needed to establish a physical distance scale. This is a direct consequence of the Alcock & Paczynski (1979, AP) effect. The second has a dynamical origin, and is related to the peculiar velocity field of galaxies, which introduce an additional contribution to the measured redshifts, from which we infer distances. This is known as the redshift-space distortions effect (Kaiser, 1987, RSD).

Models for the VSF and the VGCF must take into account the distortion effects. The following expressions relate the true and apparent comoving separation vector between a void-galaxy pair, $\mathbf{r} = (r_\perp, r_\parallel)$ and $\mathbf{s} = (s_\perp, s_\parallel)$, due to the RSD effect[*]:

$$s_\perp = r_\perp, \qquad s_\parallel = r_\parallel + v_\parallel \frac{1+z}{H(z)}, \qquad (1)$$

where $\mathbf{v} = (v_\perp, v_\parallel)$ is their relative velocity. Here, H is the Hubble parameter, and z, the redshift of the galaxy. Moreover, the subindices $\perp$ and $\parallel$ indicate the directions perpendicular to and along the line of sight (LOS). The coordinate system spanned by $\mathbf{r}$ is referred to as real space (r-space); the one spanned by $\mathbf{s}$, as redshift space (z-space).

Actually, the distance between a void-galaxy pair must be inferred from an angle θ on the plane of the sky (POS), and a redshift separation $\zeta = \Delta z$ along the LOS. This involves the following cosmological transformations:

$$s_\perp = D_\mathrm{M}(z)\theta, \qquad s_\parallel = \frac{c}{H(z)}\zeta, \qquad (2)$$

where c denotes the speed of light, and D_M, the comoving angular diameter distance. Eq. (2) accounts for the AP effect. In a flat-ΛCDM Universe, H and D_M are related and depend on the so-called background cosmological parameters: H_0 (Hubble constant), Ω_m (today's matter fraction) and Ω_Λ (today's dark-energy fraction). In turn, $\Omega_\Lambda = 1 - \Omega_m$.

3. A new fiducial-free cosmological test

According to the cosmological principle, the VGCF should be simply described by a 1D profile $\xi(r)$. However, in practice, this spherical symmetry breaks into a cylindrical symmetry along the LOS axis due to the presence of spatial distortions. Therefore, it is more convenient to represent the VGCF as a 2D contour map with axes along and perpendicular to the LOS. The presence of anisotropic patterns in these maps is a clear evidence of spatial distortions. Studying and quantifying them is then a valuable source of dynamical and cosmological information.

In Correa et al. (2019), we investigated the possibility of maximising the way in which we can extract information from the anisotropic patterns observed in the correlation maps. Thus, we developed the method of the projected correlation functions.

[*]Eq. (1) is strictly valid in the absence of AP distortions.

3.1. The projected correlation functions

Our method offers three novel aspects with respect to traditional applications of the VGCF. In the first place, we propose a fiducial-free method, since correlations are directly measured in terms of the observable quantities θ and ζ without explicitly assuming a fiducial cosmology: $\xi(\theta, \zeta)$. In this way, the AP effect is taken into account naturally.

Our method consists of projecting $\xi(\theta, \zeta)$ towards the θ-axis in a given redshift separation range PR_ζ, and towards the ζ-axis in a given angular range PR_θ. In the first case, we obtain the POS correlation function, $\xi_\mathrm{pos}(\theta)$, a 1D profile that only depends on the angular coordinate θ. In the second case, we obtain the LOS correlation function, $\xi_\mathrm{los}(\zeta)$, a 1D profile that only depends on the redshift coordinate ζ.

The second novel aspect is related to the fact of working on this observable space spanned by the coordinates (θ, ζ) and also considering two perpendicular projections of the VGCF. This allows us to effectively break any possible degeneracy in the parameter space defined by our model due to the presence of distortions.

Finally, the last aspect is related to the data covariance matrices associated with the method, which improve the Bayesian analysis to infer the model parameters. They have a notably reduced dimension compared to those obtained by considering the full correlation maps. Hence, their inversion is numerically more stable and the error propagation is substantially reduced. As a consequence, a much less number of mock catalogues is needed to estimate covariances.

By way of illustration, Fig. 2 shows the POS and LOS projections of the VGCF measured with data from the BOSS Data Release 12 (DR12) survey (points with error bars). We also show the results obtained with data from the simulated MultiDark Patchy mock surveys (Kitaura et al., 2016, curves). The consistency between both data sets is a promising result. The error bars were calculated from the covariance matrix obtained from these mocks. In both cases, we selected a void sample with sizes between $30 \leq R_\mathrm{v}/\mathrm{Mpc} \leq 35$. We took the following projection ranges: $\mathrm{PR}_\theta = 0.0232$ and $\mathrm{PR}_\zeta = 0.0131$, chosen to be approximately equal to 30 Mpc in the fiducial cosmology of the mocks. This allows us to effectively capture the anisotropic patterns in both directions.

3.2. Modeling the correlation function

The 2D correlation function can be modelled with the so-called Gaussian streaming model (Paz et al., 2013):

$$1 + \xi(s_\perp, s_\parallel) = \int_{-\infty}^{\infty} \frac{1+\xi(r)}{\sqrt{2\pi}\sigma_v} \exp\left[-\frac{(v_\parallel - v(r)\frac{r_\parallel}{r})^2}{2\sigma_v^2}\right] dv_\parallel, \quad (3)$$

where $v(r)$ is a profile characterising the velocity field around voids, and σ_v, the velocity dispersion, taken here as a free parameter. Recall that $s_\perp$ and $s_\parallel$ are related to θ and ζ by means of Eqs. (2).

The velocity profile can be analytically derived in the linear regime:

$$v(r) = -\frac{H(z)}{(1+z)}\beta(z)\frac{1}{r^2}\int_0^r \xi(r')r'^2 dr', \qquad (4)$$
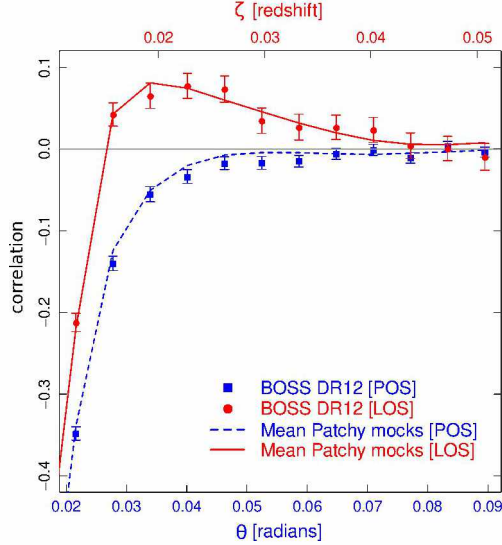
Figure 2: POS and LOS projections of the void-galaxy cross-correlation function measured with data from the BOSS DR12 survey (points with error bars) and the simulated MultiDark Patchy mocks (curves). Figure credit: Correa & Paz (2022).

where $\beta(z) = f(z)/b$, the RSD parameter, is defined as the ratio between the logarithmic growth rate of density perturbations, $f(z)$, and the bias parameter relating the galaxy and matter density fields, b.

We provided an empirical fitting expression for the r-space correlation function suitable for voids above the shot-noise level:

$$\xi(r) = \begin{cases} Ar - 1 & \text{if } r < r_{\text{wall}} \\ -\xi_0 \left[\left(\frac{r}{r_0}\right)^{-3} + \left(\frac{r}{r_0}\right)^{-\alpha} \right] & \text{if } r \geq r_{\text{wall}}, \end{cases} \quad (5)$$

where r_{wall} is a characteristic scale separating the void inner and outer parts. This model has three free parameters: ξ_0, r_0 and α (the slope A can be derived from Δ_{id}; see Correa et al. 2019).

Finally, it is important to consider that correlations are measured via a binning scheme, where several scales are mixed. A generic bin is a cylindrical shell oriented along the LOS with the following dimensions: $s_\perp^{\text{int}}$ (internal radius), $s_\perp^{\text{ext}}$ (external radius), $s_\parallel^{\text{low}}$ (lower height) and $s_\parallel^{\text{up}}$ (upper height). Then, the correlation estimator for such a bin is given by:

$$\xi_{\text{bin}} = 2 \frac{\int_{s_\parallel^{\text{low}}}^{s_\parallel^{\text{up}}} ds_\parallel \int_{s_\perp^{\text{int}}}^{s_\perp^{\text{ext}}} s_\perp [1 + \xi(s_\perp, s_\parallel)] ds_\perp}{((s_\perp^{\text{ext}})^2 - (s_\perp^{\text{int}})^2)(s_\parallel^{\text{up}} - s_\parallel^{\text{low}})} - 1. \quad (6)$$

The projected correlations are special cases with the following limits: $s_\parallel^{\text{low}} \to 0$ and $s_\parallel^{\text{up}} \to \text{PR}_\zeta$ for the POS correlation, and $s_\perp^{\text{int}} \to 0$ and $s_\perp^{\text{ext}} \to \text{PR}_\theta$ for the LOS correlation.

3.3. Testing the method

We tested the performance of our method on data from the MXXL simulation. We measured the POS and LOS correlation functions for a sample of voids with sizes be-

tween $20 \leq R_{\text{v}}/h^{-1}\text{Mpc} \leq 25$[**]. We analysed three MXXL snapshots: $z = 0.51$, 0.99 and 1.50, assumed to be the mean redshifts of void identification. This is important in view of the sampling range of modern surveys. For the implementation, we adopted a flat-ΛCDM cosmology, fixing the value of H_0. Nevertheless, the method can be easily generalised to incorporate other models as well. The cosmological parameters of interest are Ω_m and β. In order to constrain these parameters, we implemented a Bayesian analysis based on the Markov Chain Monte Carlo technique.

Fig.3 shows the main results of this analysis: the 2D likelihood marginalisations onto the $\Omega_m - \beta$ plane for the case of a projection range of $40\ h^{-1}\text{Mpc}$. From the inner to the outermost, the coloured contour levels enclose 1σ (68.3%), 2σ (95.5%) and 3σ (99.7%) confidence regions. The dashed lines indicate the respective MXXL values, whereas the white crosses, the best fitted values. Note that the target values fall inside the confidence regions in all cases, the desired calibration.

4. Redshift-space effects in voids

Observational measurements of the VSF and the VGCF show prominent deviations and anisotropic patterns that cannot be described with the standard picture of spatial distortions around voids. Traditionally, attention was paid only to the spatial distribution of the surrounding galaxies, without taking into account the impact that distortions have on some intrinsic statistical properties of voids. This is a source of additional systematics that lead to biased cosmological constraints if they are not properly modelled.

In Correa et al. (2021), we addressed this problematic. Using our spherical void finder, we aimed to find a physical connection between the r-space and z-space void populations. Essentially, we aimed to understand how voids are transformed when they are mapped from r-space into z-space. It is worth mentioning that this is not the unique way to tackle this problematic; see for instance the reconstruction technique (Nadathur et al., 2019, 2020), which approximately recovers the r-space position of galaxies before applying the void finding step. However, this method loses valuable structural and dynamical information about voids, which can be otherwise exploited by the analysis that we propose.

The analysis of the z-space mapping of galaxies is straightforward, since they can be considered as particles that are totally conserved, only their position changes (Eq. 1). The case of voids, by the contrary, is more difficult, mainly because they are extensive regions. Therefore, it is possible that some voids are destroyed under this mapping, whereas other artificial ones are created. Nevertheless, an analysis of this type is still possible. For a detailed description, I invite the reader to check our paper. In this section, I will summarise the main results.

[**]This analysis was performed with r-space voids and z-space tracers (see Correa et al. 2019 and Sec. 4 for a justification).
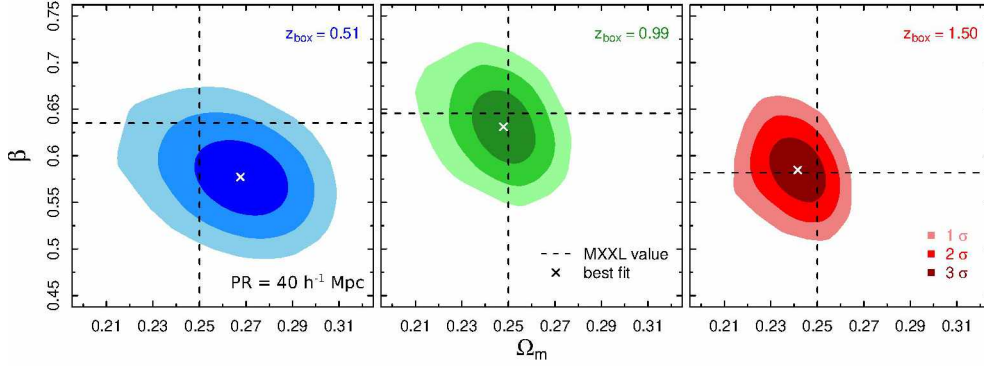
Figure 3: Calibration of our cosmological test on MXXL data for three redshifts: $z = 0.51$, 0.99 and 1.50, and for a projection range of 40 h^{-1}Mpc. The 2D likelihood distributions onto the plane $\Omega_m - \beta$ are shown. The coloured contour levels enclose 1, 2 and 3σ confidence regions. The dashed lines indicate the respective MXXL target values, whereas the white crosses are the best fitted values. Figure credit: Correa et al. (2019).
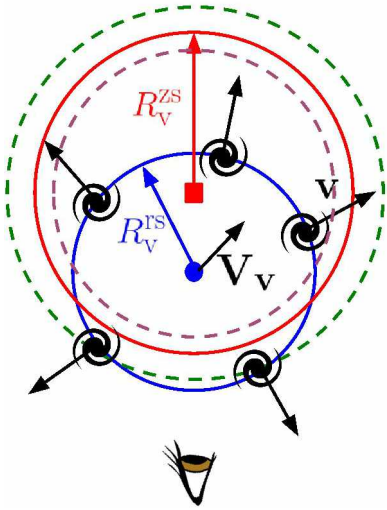

Figure 4: Schematic illustration of the the redshift-space effects in voids explained in Section 4.1.

4.1. Theoretical description

A visual impression of what happens under the z-space mapping of voids can be obtained by looking at Fig. 1. There, r-space voids are represented in blue and z-space voids in red. Fig. 4 illustrates this process schematically. We start by considering a generic spherical r-space void of radius $R_{\rm v}^{\rm rs}$, represented by the blue circle with some galaxies around. The LOS direction is assumed vertical.

- **Void number conservation.** Each r-space void identified above the shot-noise level has a unique z-space counterpart spanning the same region of space. This means that voids are conserved under the z-space mapping: each pair of voids represents the same physical entity. This also means that any difference in the statistical properties between both void populations can only be attributed to the AP and RSD effects acting under this mapping.
- **Expansion effect.** Voids appear elongated along the LOS in z-space. This is a consequence of the classic RSD induced by tracer dynamics at scales near the void radius. However, as our void finder

identifies spherical rather ellipsoidal regions, the net effect is an expanded sphere in z-space, as illustrated in the figure by the red circle. This expansion effect imprints a distortion pattern on observations that we denote as t-RSD.

- **AP-volume effect.** The volume of voids is also affected by the AP effect. However, unlike the previous effect, the net effect here can be an expansion or a contraction, it all depends on the selected fiducial cosmology. This is illustrated in the figure by the green and purple circles.
- **Combined effects.** We found a simple relation for void radii in z-space, $R_{\rm v}^{\rm zs}$, and r-space, $R_{\rm v}^{\rm rs}$, that take into account the combined t-RSD and AP-volume effects:

$$R_{\rm v}^{\rm zs} = q_{\rm AP} \, q_{\rm RSD} \, R_{\rm v}^{\rm rs}. \tag{7}$$

On the one hand,

$$q_{\rm RSD} = 1 - \frac{1}{6}\beta(z)\Delta_{\rm id}, \tag{8}$$

a constant factor encoding the t-RSD effect derived from the basis of Eq. (4). Note that $q_{\rm RSD} > 1$ always (since $\Delta_{\rm id} < 0$), in agreement with an expansion. Note also that it only depends on the cosmological parameter β. On the other hand,

$$q_{\rm AP} = \sqrt[3]{\left(\frac{D_{\rm M}^{\rm fid}(z)}{D_{\rm M}^{\rm rs}(z)}\right)^2 \frac{H^{\rm rs}(z)}{H^{\rm fid}(z)}}, \tag{9}$$

a constant factor encoding the AP-volume effect derived from the basis of Eqs. (2). Here, the superscripts "rs" and "fid" refer to real and fiducial quantities, respectively. Note that it only depends on the background cosmological parameters.

- **Off-centring effect.** Void centres are systematically shifted along the LOS in z-space, as also illustrated in the figure. This effect can be understood by considering that the whole void region coherently moves through space with a net velocity $\mathbf{V_v}$ (Lambas et al., 2016). This is a consequence of a new class of RSD induced by the global void dynamics, which can be quantified by the same RSD-shift expression of Eq. (1) but applied to the case of voids:

$$s_{\rm v\perp} = r_{\rm v\perp}, \qquad s_{\rm v\parallel} = r_{\rm v\parallel} + V_{\rm v\parallel}\frac{1+z}{H(z)}. \tag{10}$$

Here, $\mathbf{r}_v = (r_{v\perp}, r_{v\parallel})$, $\mathbf{s}_v = (s_{v\perp}, s_{v\parallel})$ and $\mathbf{V}_v = (V_{v\perp}, V_{v\parallel})$ denote the r-space and z-space position vectors of the centre, and the void net velocity, respectively. This off-centring effect imprints a distortion pattern on observations that we denote as v-RSD.

- **Independence of the effects.** All the mentioned effects are independent from each other. This means that they can be modelled separately.
- **Ellipticity effect.** This is an additional effect that only manifests on measurements of the VGCF (not represented schematically in the figure). Voids are intrinsically ellipsoidal rather than spherical (in r-space). This is a source of an additional anisotropic pattern, which we denote as e-RSD.

4.2. Statistical analysis

We provided a thorough statistical analysis to demonstrate all the effects described here. The main results are shown in Fig. 5. The left-hand panel shows the VSF of the MXXL simulation for both spatial configurations: r-space in blue and z-space in red. The solid curves correspond to the full void sample. The dashed curves correspond to the subset of those voids that are conserved under the z-space mapping. The vertical line represents the median of the distribution, and is an indicator of the shot-noise level. Voids below this level are spurious and must not be taken into account. The fact that the solid and dashed curves tend to be the same above this level is an indicator that it is valid to assume void number conservation. The central panel shows the 2D distribution between R_v^{rs} and R_v^{zs} as a heat map. There is a linear trend well described by Eq. (7) (black solid line), a demonstration of the expansion effect described above (for this particular analysis $q_{\mathrm{AP}} = 1$, since we worked on the true cosmological framework of the simulation). The right-hand panel shows the 2D distribution between $V_{v\parallel}$ and $d_{v\parallel}$, i.e. the LOS components of the void net velocity and the displacement of the centres (normalised to the void radius). There is a linear trend well described by Eq. (10) (black dashed line), a demonstration of the off-centring effect described above.

Fig. 6 shows the impact of the z-space effects in voids on the VSF. The left-hand panel shows the void abundance of the MXXL in four different situations: in r-space (blue solid), z-space with the true MXXL cosmology (red solid), z-space with a fiducial cosmology chosen such that $\Omega_m < \Omega_m^{\mathrm{MXXL}}$ (green dot-dashed), and z-space with a fiducial parameter $\Omega_m > \Omega_m^{\mathrm{MXXL}}$ (purple dashed). Note that the first two are the same curves shown in Fig. 5, but in the range above the shot-noise level. The last two mimic two possible observational measurements. The goal is to correct these abundance curves in order to recover the true underlying one in r-space. This can be achieved by means of Eq. (7). As two factors are involved in this expression, the correction can be performed in two steps: first applying q_{AP} for the AP-volume effect, and then q_{RSD} for the expansion effect. This is shown in the central and right-hand panels, respectively. In the first step, the fiducial abundances are corrected and the red solid curve is recovered. In the

second step, the blue solid curve is recovered. The lower panels show the relative differences between the curves before and after each correction, respectively. This analysis reinforces the validity of the t-RSD and AP-volume effects, but also shows that they can be treated independently.

The ellipticity effect demands a detailed and long analysis to be explained. For this reason, I will not cover it in this article. I invite the reader to see Correa et al. (2022) for more details.

5. Conclusions

In this era of high-precision cosmological measurements, cosmic voids are promising cosmological probes for studying the dark-energy problem and alternative gravity theories. The VSF and the VGCF are two powerful void statistics for the design of cosmological tests. However, a complete description of the effects of spatial distortion around voids is necessary. The AP and RSD effects do not only affect the spatial distribution of the surrounding galaxies, they also affect intrinsic void properties, such as their size and spatial distribution. This is a source of additional systematics that lead to biased cosmological constraints if they are not properly modelled.

In this article, I presented a theoretical framework to address this problematic based on a cosmological and dynamical analysis of the mapping of voids between r-space and z-space. A central aspect is that voids identified above the shot-noise level are conserved. Based on this result, we found three effects that act on them altering their properties: (i) a systematic expansion due to tracer dynamics (t-RSD), (ii) a systematic off-centring due to void dynamics (v-RSD), and (iii) a volume change due to the AP effect. We also found a fourth source of anisotropic patterns on the VGCF, the ellipticity effect (e-RSD). It is essential that models for the VSF and the VGCF take all of them into account in order to obtain unbiased cosmological constraints. These effects are not only important for cosmological purposes, they can also shed light about important structural and dynamical properties of voids.

In addition, I presented a new cosmological test based on the VGCF, which offers three novel aspects: (i) it is based on two perpendicular projections of the correlation function, (ii) it is fiducial-cosmology free, which allows us to effectively break any possible degeneracy between the cosmological parameters, and (iii) it allows us to significantly reduce the number of mock catalogues needed to estimate covariances.
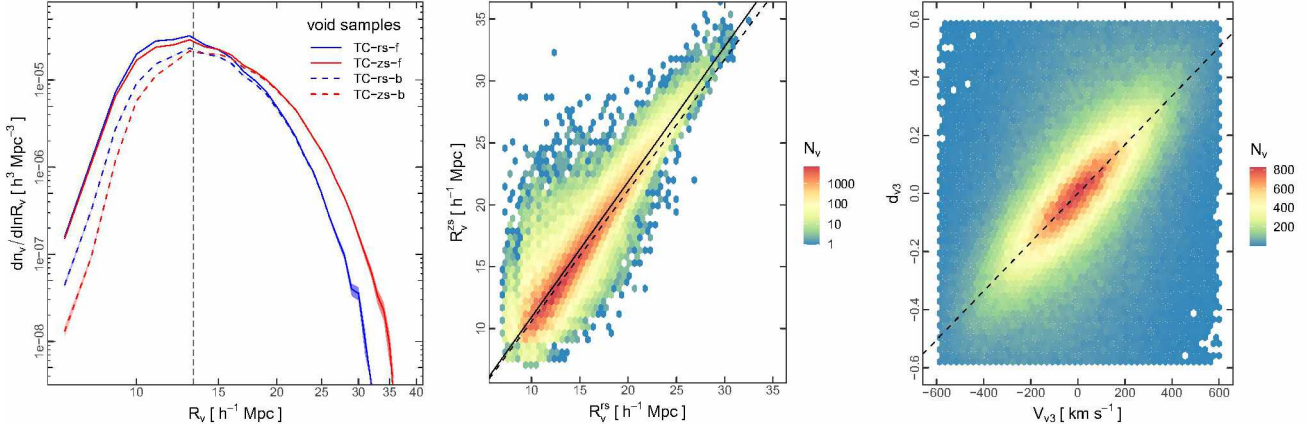
Figure 5: *Left-hand panel:* void abundance of the MXXL simulation measured in real (blue) and redshift (red) space. Conserved voids (dashed curves) tend to the full sample (solid curves) above the shot-noise level (vertical line), so both are indistinguishable. *Central panel:* 2D distribution between void radii in both spatial configurations. *Right-hand panel:* 2D distribution between the LOS void-net velocity and centre displacement. The linear trends are a statistical demonstration of the expansion and off-centring effects, respectively. Figure credit: Correa et al. (2021).
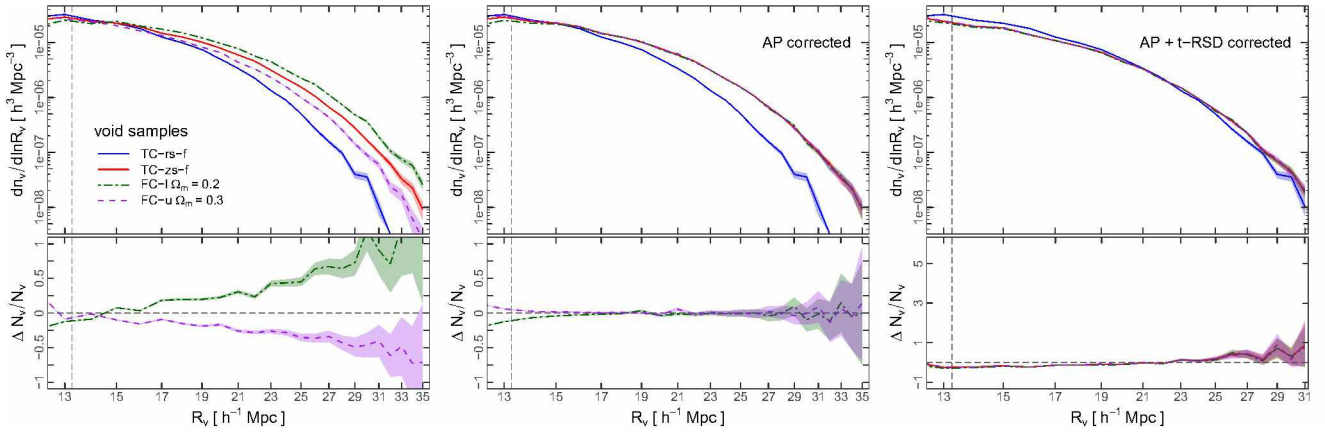

Figure 6: Impact of the z-space effects in voids on the VSF. *Left-hand panel:* void abundance of the MXXL in four different situations: r-space (blue solid), MXXL z-space (red solid), fiducial z-space with $\Omega_m < \Omega_m^{\mathrm{MXXL}}$ (green dot-dashed), and fiducial z-space with $\Omega_m > \Omega_m^{\mathrm{MXXL}}$ (purple dashed). *Central and right-hand panels:* VSF two-step correction for the volume effects. *Lower panels:* relative differences between the curves before and after each correction. Figure credit: Correa et al. (2021).

References

Alcock C., Paczynski B., 1979, Nature, 281, 358
Angulo R.E., et al., 2012, MNRAS, 426, 2046
Cai Y.C., et al., 2016, MNRAS, 462, 2465
Contarini S., et al., 2022, A&A, 667, A162
Correa C.M., Paz D.J., 2022, BAAA, 63, 193
Correa C.M., et al., 2019, MNRAS, 485, 5761
Correa C.M., et al., 2021, MNRAS, 500, 911
Correa C.M., et al., 2022, MNRAS, 509, 1871
Dawson K.S., et al., 2013, AJ, 145, 10
Furlanetto S.R., Piran T., 2006, MNRAS, 366, 467
Hamaus N., et al., 2020, JCAP, 2020, 023
Hamaus N., et al., 2022, A&A, 658, A20
Hawken A.J., et al., 2020, JCAP, 2020, 012
Hill G.J., et al., 2008, T. Kodama, T. Yamada, K. Aoki (Eds.), *Panoramic Views of Galaxy Formation and Evolution, Astronomical Society of the Pacific Conference Series*, vol. 399, 115
Jennings E., Li Y., Hu W., 2013, MNRAS, 434, 2167

Kaiser N., 1987, MNRAS, 227, 1
Kitaura F.S., et al., 2016, MNRAS, 456, 4156
Lambas D.G., et al., 2016, MNRAS, 455, L99
Laureijs R., et al., 2011, arXiv e-prints, arXiv:1110.3193
Levi M., et al., 2019, *BAAS*, vol. 51, 57
Nadathur S., Carter P., Percival W.J., 2019, MNRAS, 482, 2459
Nadathur S., et al., 2020, MNRAS, 499, 4140
Neyrinck M.C., 2008, MNRAS, 386, 2101
Padilla N.D., Ceccarelli L., Lambas D.G., 2005, MNRAS, 363, 977
Paz D., et al., 2013, MNRAS, 436, 3480
Paz D.J., et al., 2022, arXiv e-prints, arXiv:2212.06849
Planck Collaboration, et al., 2020, A&A, 641, A6
Ruiz A.N., et al., 2015, MNRAS, 448, 1471
Sánchez A.G., et al., 2013, MNRAS, 433, 1202
Sheth R.K., van de Weygaert R., 2004, MNRAS, 350, 517
Suzuki N., et al., 2012, ApJ, 746, 85